ACS APPLIED MATERIALS & INTERFACES

Research Article

www.acsami.org

Novel Approach for Developing Dual-Phase Ceramic Membranes for Oxygen Separation through Beneficial Phase Reaction

Zhenbao Zhang,[†] Wei Zhou,[†] Yubo Chen,[†] Dengjie Chen,[§] Jiawei Chen,[†] Shaomin Liu,[‡] Wanqin Jin,[†] and Zongping Shao*[,†,‡]

[†]State Key Laboratory of Materials-Oriented Chemical Engineering, College of Chemistry & Chemical Engineering, Nanjing Tech University, Nanjing 210009, P. R. China

[‡]Department of Chemical Engineering, Curtin University, Perth, Western Australia 6845, Australia

[§]Department of Chemistry, Jinan University, Guangzhou 510632, P.R. China

Supporting Information

ABSTRACT: A novel method based on beneficial phase reaction for developing composite membranes with high oxygen permeation flux and favorable stability was proposed in this work. Various $Ce_{0.8}Sm_{0.2}O_{2-\delta}$ (SDC) + $SrCO_3$+Co_3O_4 powders with different SDC contents were successfully fabricated into membranes through high temperature phase reaction. The X-ray diffraction (XRD) measurements suggest that the solid-state reaction between the SDC, $SrCO_3$ and Co_3O_4 oxides occurred at the temperature for membrane sintering, leading to the formation of a highly conductive tetragonal perovskite phase $Sm_xSr_{1-x}CoO_{3-\delta}$. The morphology and elemental distribution of the dual-phase membranes were characterized using back scattered scanning electron microscopy and energy dispersive X-ray spectroscopy (BSEM-EDX). The oxygen bulk diffusivity and surface exchange properties of the materials were investigated via the electrical conductivity relaxation technique, which supported the formation of conductive phases. The SDC+20 wt % $SrCO_3$+10.89 wt % Co_3O_4 membrane exhibited the highest permeation flux among the others, reaching 0.93 mL cm^{-2} min^{-1} [STP = standard temperature and pressure] under an air/helium gradient at 900 °C for a membrane with a thickness of 0.5 mm. In addition, the oxygen permeation flux remained stable during the long-time test. The results demonstrate the beneficial phase reaction as a practical method for the development of high-performance dual-phase ceramic membranes.

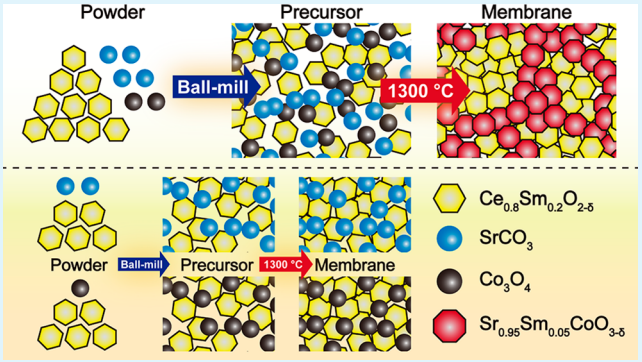

KEYWORDS: *oxygen permeation, phase reaction, permeation flux, stability, dual-phase membrane*

1. INTRODUCTION

Oxygen is an important raw material in modern society with an annual production of 100 million tons, and currently, the smelting of iron ore in the steel and chemical industries consumes 55% and 25%, respectively, of commercially produced oxygen.[1] Other application fields of oxygen include medical applications, metal cutting and welding, oxidizers in rocket fuel, and water treatment. Very recently, the oxyfuel process has attracted interest for reducing emissions and easy subsequent CO_2 sequestration.[2,3] The success of this innovative technology may result in a substantial increase in oxygen demand, while economic separation of oxygen from air becomes the most critical point. This is because conventional oxygen production based on the cryogenic distillation of air requires a large amount of energy, accounting for nearly 15% of the total energy consumption of a coal-fired power station.[4,5]

Oxygen separation via mixed conducting membranes has emerged as a new advanced technology that enables the separation of oxygen from an oxygen-containing atmosphere at elevated temperature under the driving force of an oxygen partial pressure gradient across the membranes.[6,7] This process features infinite oxygen selectivity, low energy consumption, continuous operation, and the capability to be integrated with an oxidative chemical reaction (such as the partial oxidation of methane into a synthesis gas).[8−11] In the early development stage, mixed conducting membranes were fabricated mainly from ceramic-precious metal composites, where the ceramic phase was a pure oxygen-ion conductor, mainly yttria-stabilized zirconia (YSZ) and Bi_2O_3-based oxides, which provided the oxygen-ion conducting path in the composite membrane, while a precious metal acted as the electronic conductor.[12−15] To form continuous diffusion paths for both oxygen ions and electrons inside the membrane bulk, both phases should be formed in a percolating way. Therefore, the volume content of

Received: June 29, 2015
Accepted: September 29, 2015
Published: September 29, 2015

DOI: 10.1021/acsami.5b05812
ACS Appl. Mater. Interfaces 2015, 7, 22918−22926

the precious metal is typically greater than 28%, which makes such composite membranes very expensive. In addition, the membranes generally have low oxygen permeability with an oxygen flux less than 0.1 mL cm^2 min^{-1} [STP = standard temperature and pressure] at 900 °C.[16,17] Later, single-phase oxides that possessed mixed oxygen-ion and electronic conductivity were developed for constructing ceramic membranes for oxygen separation. These membranes usually exhibit much higher oxygen permeability than conventional dual-phase membranes with permeation fluxes of up to 3.0 mL min^{-1} cm^{-2} [STP] under an air/helium oxygen gradient.[18−20] Among these materials, mixed conducting perovskite oxides have received particular attention because of their high oxygen-ion conductivity in addition to ultrahigh electronic conductivity up to 2000 S cm^{-1}.[21,22] Unfortunately, these single-phase ceramic membranes show significant disadvantages such as insufficient phase stability, easy poisoning by CO_2, and poor mechanical strength.[23,24]

Because of their superior chemical and mechanical stabilities, dual-phase membranes have recently attracted increasing interest from the scientific community. Considering the high price of precious metals, a general trend is to apply an electronic conducting oxide as a replacement. For example, Li and colleagues fabricated $Zr_{0.84}Y_{0.16}O_{1.92}$ (YSZ) + $La_{0.8}Sr_{0.2}MnO_{3-\delta}$ (LSM) composite hollow-fiber membranes with a wall thickness of 0.16 mm for oxygen separation, which reached the permeation flux of 0.28 mL min^{-1} cm^{-2} [STP] at 950 °C.[25] Since the mobility of oxygen ions is much lower than electrons, maximizing the apparent oxygen-ion conductivity in the dual-phase membranes is a preferred approach to improving the oxygen permeation flux. Thus, the portion of the electronic conducting phase in the dual-phase membrane should be as small as possible if its percolating manner is still met. Special morphological control is usually required to minimize the use of the electronic conducting phase in the composite, which makes the fabrication a complicated process.

Very recently, a new concept of mixing a highly oxygen-ionic conductive phase, such as doped ceria and a mixed conducting perovskite phase with large electronic conductivity was proposed for the development of ceramic membranes for oxygen separation.[26] Such membranes ensure high oxygen-ion conductivity since both phases are high oxygen ionic conductors. The ionic conducting phase can be YSZ, doped ceria or $La_{0.9}Sr_{0.1}Ga_{0.8}Mg_{0.2}O_{3-\delta}$ (LSGM), which possesses high ionic conductivity at elevated temperature, and the other phase is typically a mixed conducting perovskite oxide, such as $La_{0.6}Sr_{0.4}Co_{0.2}Fe_{0.8}O_{3-\delta}$ (LSCF).[27−30] In solid oxide fuel cells (SOFCs), interfacial reaction between cell components should be avoided because such a reaction usually results in the formation of an insulating phase, which will have a detrimental effect on the charge transfer and consequently on the cell performance. The same selection strategy has also often been applied for the two phases in such dual-phase membranes.[31,32] Recently, we demonstrated that by carefully tailoring the composition, this type of interfacial reaction may also provide a beneficial effect on the electrode performance in SOFCs.[33] The cations' interdiffusion between different phases in a composite electrode during high-temperature calcination could lead to the formation of a new phase, which exhibited much improved electrochemical activity for the oxygen reduction reaction.

Herein, we report a novel approach for the development of dual-phase ceramic membranes for oxygen separation with favorable oxygen permeability and stability by utilizing the beneficial phase reaction at high temperature. Instead of the pre-synthesis of the mixed conducting perovskite oxide as the starting material for the fabrication of the composite membrane, we used a parent oxides or even raw materials for this perovskite oxide. A solid-state reaction between the oxygen-ion conducting phase (SDC) and the raw materials ($SrCO_3$ + Co_3O_4) of the perovskite phase occurred during the high-temperature fabrication, resulting in the formation of a highly conductive tetragonal perovskite phase $Sm_xSr_{1-x}CoO_{3-\delta}$, which also functioned as a sintering aid to enable a dense membrane to be obtained at lower fabrication temperature. By using this innovative beneficial phase reaction technique, the dual-phase membrane with high oxygen permeation flux and favorable stability could be developed for oxygen separation.

2. EXPERIMENTAL SECTION

2.1. Preparation of Powders and Membranes. $Ce_{0.8}Sm_{0.2}O_{2-\delta}$ (SDC) powder was synthesized through a combined citrate and EDTA complexing sol−gel process, and the detailed synthesis procedure is described elsewhere.[34] Various SDC + $SrCO_3$ + Co_3O_4 precursor powders with different SDC contents (the mole ratio of $SrCO_3/Co_3O_4$ is fixed at 3:1) were prepared by a high-energy ball-milling method using SDC, $SrCO_3$, and Co_3O_4 oxide as the raw materials for the metal sources. Starting raw materials were mixed by high-energy ball milling (Fritsch, Pulverisette 6) at a rotation speed of 400 rpm for 40 min with ethanol as the liquid medium. After drying, the powder mixture was compressed into disk-shaped membranes in a stainless steel mold (15.0 mm in diameter) under hydraulic pressure of approximately 1.5×10^8 Pa, followed by sintering at 1300 °C for 10 h in air. For comparison, the SDC + $SrCoO_{3-\delta}$ membrane was synthesized using a similar procedure; the $SrCoO_{3-\delta}$ oxide was pre-synthesized, and calcined at a lower temperature of 1200 °C for 10 h. Listed in Table 1 are the as-synthesized samples with Sample number and corresponding sintering temperature.

Table 1. Sample Number and Corresponding Sintering Temperature for the As-Synthesized Samples

sample composition	sample no.	sintering temperature
SDC + 40 wt % $SrCO_3$ + 21.76 wt % Co_3O_4 precursor powders	I	none
SDC + 10 wt % $SrCO_3$ + 5.44 wt % Co_3O_4	II	1300 °C
SDC + 20 wt % $SrCO_3$ + 10.89 wt % Co_3O_4	III	1300 °C
SDC + 40 wt % $SrCO_3$ + 21.76 wt % Co_3O_4	IV	1300 °C
SDC + 26.36 wt % $SrCoO_{3-\delta}$ precursor powders	V	none
SDC + 26.36 wt % $SrCoO_{3-\delta}$	VI	1200 °C
SDC + 20 wt % $SrCO_3$	VII	1300 °C
SDC + 10.89 wt % Co_3O_4	VIII	1300 °C

2.2. Characterizations. The crystal structures of the as-prepared precursor powders and dual phase membranes were examined by X-ray diffraction (XRD) using a Bruker D8 Advance diffractometer in the range of 2θ from 20 to 80° with intervals of 0.02°. Rietveld refinements of the XRD patterns were performed using GSAS software. The dual-phase membranes were observed using back scattered scanning electron microscopy (BSEM, NEON 40EsB) and energy dispersive X-ray spectroscopy (EDX, EDAX GENESIS 2000) elemental mapping was used to clarify the elemental distribution. Accurate elements composition of as-prepared membranes was determined by wavelength-dispersive X-ray spectroscopy (WDS, XRF ARL-9800).

The electrical conductivities of the as-synthesized samples in air were measured using a four-probe DC technique on the sintered bars within the temperature range of 300−900 °C at an interval of 25 °C, which was described in detail in our previous paper.[35] Electrical conductivity relaxation (ECR) was used to determine the chemical

DOI: 10.1021/acsami.5b05812
ACS Appl. Mater. Interfaces 2015, 7, 22918−22926

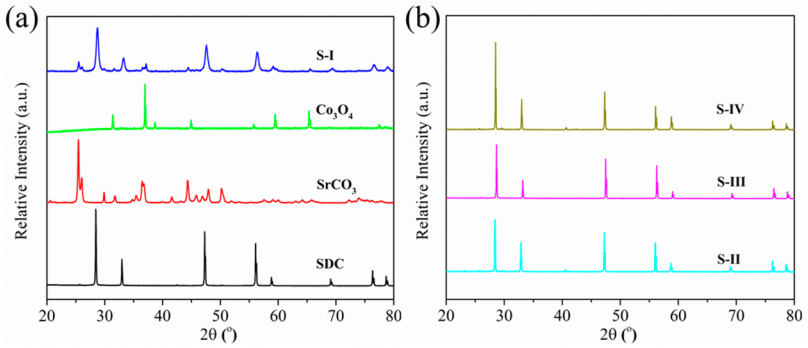

Figure 1. XRD patterns of SDC, $SrCO_3$, Co_3O_4, a typical mixture of SDC + $SrCO_3$ + Co_3O_4 (**S−I**) after ball milling without sintering (a) and SDC + 10 wt % $SrCO_3$ + 5.44 wt % Co_3O_4 (**S−II**), SDC + 20 wt % $SrCO_3$ + 10.89 wt % Co_3O_4 (**S−III**), SDC + 40 wt % $SrCO_3$ + 21.76 wt % Co_3O_4 (**S−IV**) membranes after sintering at 1300 °C for 10 h (b).

bulk diffusion coefficient (D_{chem}) and chemical surface exchange coefficient (κ_{chem}) with the bar-shaped dual-phase pellets. Measurements were performed over a temperature range of 650−850 °C at an interval of 50 °C. The oxygen partial pressure in the surrounding atmosphere of the bar-shaped samples was achieved by the introduction of O_2 and Ar gas mixtures with quantitative oxygen content. After the bar-shaped pellets were stabilized at a certain temperature under a controlled atmosphere, the oxygen partial pressure of the samples was abruptly switched from 0.10 to 0.21 atm. The time dependence of the conductivity was measured using the four-probe DC technique. After every change of the oxygen pressure, the bar was stabilized for at least 1 h before the next data were collected using a digital source meter (Keithley 2420). The values of D_{chem} and κ_{chem} of the bar-shaped sample were obtained from the electrical conductivity relaxation curves by ECRTOOLS.[36,37]

2.3. Oxygen Permeation Flux Measurement. The oxygen permeation fluxes through the as-prepared dual phase membranes were measured in the temperature range of 700−950 °C. The membranes were polished on both sides to a thickness of 0.5 mm using 400 mesh SiC abrasive paper and then sealed on a dense Al_2O_3 tube with the silver paste used as sealant. To avoid radical contribution to the oxygen flux, the sidewall of the membranes was also covered with the silver. One side of the disk-shaped membranes was exposed to the ambient air, which was applied as the oxygen-rich side atmosphere; the other side was swept with helium with the flow of 100 mL min^{-1} [STP] to create the oxygen pressure gradient across the membrane. The composition of the permeated effluent gas was determined using a gas chromatograph (GC, Varian CP-3800) equipped with a thermal conductivity detector (TCD) and a 5 Å capillary molecule column for quantitative concentration analysis. The oxygen permeation flux from leakage through the silver sealant was corrected by determining the N_2 concentration in the permeated gas. During the measurement, membranes with relative densities of higher than 95% were used for oxygen permeation test.

Subsequently, an **S−III** membrane was subjected to the long-term oxygen permeation testing; one side of the membrane was exposed to ambient air while the other side was swept with a pure CO_2 stream at a constant flow rate of 30 mL min^{-1} [STP]. A thick membrane with thickness of 1.2 mm was adopted to minimize the role of surface exchange in the rate determination of the oxygen permeation flux.

3. RESULTS AND DISCUSSION

3.1. Phase Composition. Figure 1 presents the XRD patterns of SDC, $SrCO_3$, Co_3O_4, a typical mixture of SDC + $SrCO_3$ + Co_3O_4 precursor powder after ball-milling without sintering, and the various SDC + $SrCO_3$ + Co_3O_4 (fixed $SrCO_3/Co_3O_4$ weight radio) membranes with different SDC contents after the sintering at 1300 °C for 10 h; After the high-temperature calcinations, the characteristic diffraction peaks for $SrCO_3$ and Co_3O_4 completely disappeared for the various SDC + $SrCO_3$ + Co_3O_4 samples with different $SrCO_3$ + Co_3O_4 contents; the diffraction patterns could be indexed based on a mixture of cubic fluorite phase and a tetragonal perovskite phase. To further examine the exact chemical composition of as-sintered dual-phase membranes, XRF-WDS measurement of the crushed membrane powders was performed, and the result is displayed in Table S1.

To obtain a more in-depth understanding about the phase reaction in the mixtures during the high-temperature calcinations, we selected the **S−III** membrane as a representative sample, for which the XRD patterns of the disk-shaped sample after the sintering at 1300 °C for 10 h was subjected to Rietveld refinement, with the results shown in Figure 2a. For comparison, XRD characterization and Rietveld

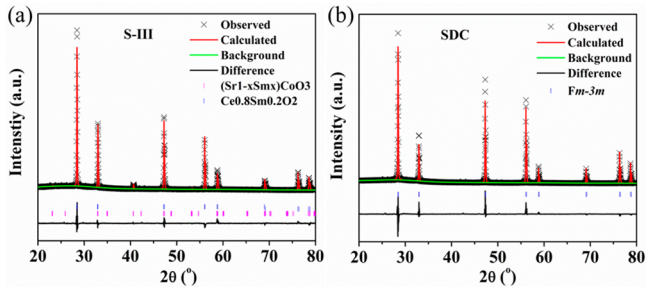

Figure 2. XRD patterns with Rietveld refinement plots of SDC + 20 wt % $SrCO_3$ + 10.89 wt % Co_3O_4 (**S−III**) (a) and SDC (b) membranes.

refinement of the pattern for SDC, calcined at 1300 °C for 10 h, were also conducted. Figure 2b shows the XRD pattern and refinement plots of the calcined SDC membrane. The XRD pattern can be refined based on a cubic fluorite structure with space group $Fm\bar{3}m$, $a = b = c = 5.436(1)$ Å. The results agree well with the literature for $Sm_{0.2}Ce_{0.8}O_{1.9}$.[38] For the calcined **S−III** sample, the XRD diffraction pattern can be refined based on a mixture of 72.1 wt % cubic fluorite phase SDC with space group $Fm\bar{3}m$, $a = b = c = 5.442(4)$ Å and 27.9 wt % of a tetragonal perovskite phase $Sr_{1-x}Sm_xCoO_{3-\delta}$ with space group $P4/mmm$, $a = b = 3.845(6)$ Å, $c = 7.709(4)$ Å, $V = 114.0(1)$ $Å^3$ (assuming $x = 0.05$). The low error $R_{wp} = 4.30\%$, $R_p = 2.77\%$, and $\chi^2 = 6.228$ also indicates the good fitting. The smaller lattice parameter of the pristine SDC compared with that of the fluorite phase in the composite after the calcinations suggests partial Sm in SDC may be lost after the calcinations process. This agrees well with the result of our previous study that

DOI: 10.1021/acsami.5b05812
ACS Appl. Mater. Interfaces 2015, 7, 22918−22926

cation exchange between SDC and $SrCoO_{3-\delta}$ occurs at elevated temperature.[33] Previously, we demonstrated that a small amount of Sm doping into the Sr site of $SrCoO_{3-\delta}$ greatly facilitated the formation of oxygen vacancy-disordered perovskite.[21] This finding suggests that partial Sm was diffused from the SDC phase to react with $SrCO_3$ and Co_3O_4 with the formation of $Sm_xSr_{1-x}CoO_{3-\delta}$ perovskite, in good agreement with the XRD results. The concentration of Sm is around 5% as compared with the structural parameters of $Sr_{0.95}Sm_{0.05}CoO_{3-\delta}$ (Figure S1a) and $Sr_{0.9}Sm_{0.1}CoO_{3-\delta}$ (Figure S1b). The weight ratio of the perovskite phase in the sintered product should be approximately 26.9 wt %, which is very close to the refined result of 27.9 wt % determined by Rietveld refinement of the XRD pattern. This result further supported the successful formation of the $Sr_{0.95}Sm_{0.05}CoO_{3-\delta}$-type oxide in the **S−III** sample after the calcinations at 1300 °C.

We also conducted compositional and phase analysis of the **S−VI** membrane after the sintering at 1200 °C, based on Rietveld refinement of XRD Patterns (Figure S2). Notably, three phases could be distinguished from the XRD pattern of **S−VI** sample: SDC, the tetragonal perovskite $Sm_xSr_{1-x}CoO_{3-\delta}$ and the K_2NiF_4-type phase $Sm_{2-x}Sr_xCoO_{4+\delta}$ with a weight ratio of approximately 4:1. Therefore, the selection of a proper material for the various raw materials for the fabrication is critical to the in situ formation of a conductive perovskite phase inside the membrane during high-temperature sintering.

3.2. Microstructure and Element Analysis. The feasibility of the fabrication of the dual-phase membrane via beneficial phase reaction was then examined by practical membrane fabrication and subsequent BSEM observation. Shown in Figure 3a and b are typical BSEM images from

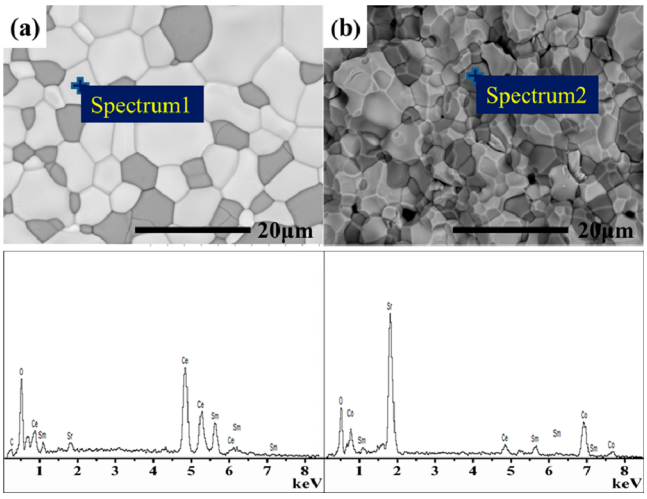

Figure 3. BSEM images of the surface (a) and cross-section (b) of the SDC + 20 wt % $SrCO_3$ + 10.89 wt % Co_3O_4 (**S−III**) membrane sintered at 1300 °C. The EDX results are indicated in the BSEM image.

surface and cross-sectional views, respectively, of the **S−III** membrane sintered at 1300 °C. Two types of particles with size of 1−5 μm but different color contrasts were observed on both the surface (Figure 3a) and cross-section (Figure 3b). It suggests that the membrane was composed of two different phases. Perfect densification of the membrane was realized, as indicated by the absence of pores. It is well-known that cobalt oxide and alkaline earth oxide are good sintering aids for ceramics,[39−41] which may promote the membrane sintering in this study. The compositions of selected particles with different contrast from both the surface and cross section, as marked in the SEM images in Figure 3, were subjected for further EDX analysis with the results presented next to the BSEM images. The dark particle of the membrane surface was mainly composed of Sr and Co elements and a small amount of Sm (the atomic ratio of Sm to Sr is 1:9), while very little Ce (the atomic ratio of Ce to Sm is 1:30) was detected from those particles. These results suggest that the dark particles were composed of slightly Sm-doped $SrCoO_{3-\delta}$, that is, $Sm_{0.1}Sr_{0.9}CoO_{3-\delta}$, which corresponds to the perovskite phase with the composition of $Sm_{0.05}Sr_{0.95}CoO_{3-\delta}$ as determined by XRD analysis. The small difference in the Sm content ratio from the EDX analysis and XRD refinement for the perovskite phase (dark particles) may be due to experimental errors. The particles with brighter contrast were mainly composed of Sm and Ce elements (in addition to oxygen), thus being assigned to the SDC phase. Similar conclusions were also made by analyzing the compositions of the dark and bright particles at the cross section of the membrane, which suggests that the two phases were homogeneously distributed throughout the entire membrane.

The **S−III** membrane was further examined by conducting surface mapping of different elements to provide a clearer picture of the element distribution within the membrane. Figure 4a shows a part of SEM-EDX element mapping image of

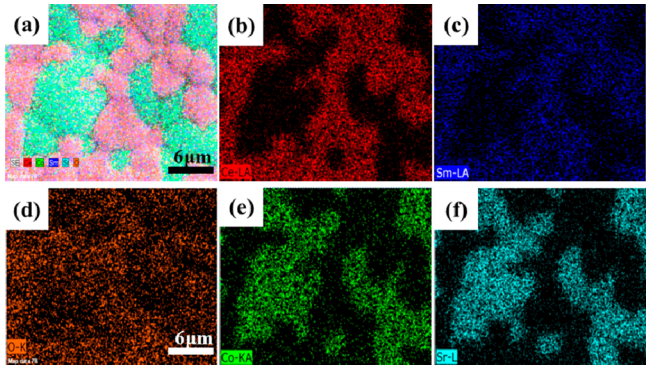

Figure 4. SEM-EDX element mapping image of the surface of the SDC + 20 wt % $SrCO_3$ + 10.89 wt % Co_3O_4 (**S−III**) membrane (a), and the corresponding EDX mapping of the various elements, Ce (b), Sm (c), O (d), Co (e), and Sr (f).

the membrane, and the corresponding element mapping images for Ce, Sm, O, Co, and Sr are presented in Figure 4b−f. The results clearly demonstrate that the membranes were composed of two different types of particles; one type is rich in Sm and Ce, and the other type is rich in Sr and Co. In combination with the XRD results, the Sm- and Ce-rich phase is the fluorite phase SDC, and the Sr- and Co-rich phase is the perovskite phase $Sm_{0.05}Sr_{0.95}CoO_{3-\delta}$. The fluorite phase SDC formed a well-connected diffusion path from the surface view, whereas the perovskite phase appears less percolating. Because the mobility of oxygen ions is much slower than electrons, the formation of a more percolating SDC phase in the composite membrane is beneficial for increasing the oxygen permeability.

3.3. Conductivity and Electrical Conductivity Relaxation. Note that the percolation is a three-dimensional phenomenon; however, the BSEM image can only provide two-dimensional information. Thus, another technique is required to obtain more accurate information about the

DOI: 10.1021/acsami.5b05812
ACS Appl. Mater. Interfaces 2015, 7, 22918−22926

percolation behavior of both phases. Under air atmosphere, SDC is a pure oxygen-ion conductor with a total conductivity of less than 0.1 S cm^{-1} at 900 °C.[42] For comparison, $Sm_{1-x}Sr_xCoO_{3-\delta}$ exhibited very high conductivity up to 500 S cm^{-1}. The formation of mutual percolating fluorite SDC and perovskite phase $Sm_{1-x}Sr_xCoO_{3-\delta}$ in the bar-shaped samples should yield an obvious increase in conductivity compared with the pure SDC or SDC + perovskite composite sample with nonpercolating perovskite phase. The total conductivity of the various samples was then measured using 4-probe DC method. Figure 5a shows the electrical conductivity of $SrCoO_{3-\delta}$, $Sm_{0.05}Sr_{0.95}CoO_{3-\delta}$ and $Sm_{0.1}Sr_{0.9}CoO_{3-\delta}$, $SrCO_3$, and Co_3O_4 at various temperatures. $SrCO_3$ bar-shaped pellet exhibited an insulating behavior with conductivity less than 0.1 S cm^{-1} even at 900 °C, and Co_3O_4 also exhibited relatively low conductivity at temperature less than 800 °C; however, a sharp increase in conductivity from 10 to 30 S cm^{-1} at the temperature range from 800 to 900 °C was observed, suggesting an accompanying phase transition. $SrCoO_{3-\delta}$ had modest conductivity varying from 8 to 29 S cm^{-1} depending on the temperature and demonstrated a semiconducting behavior, that is, an increase in conductivity with the increase of the investigated temperature range. The doping of a small amount of Sm (x = 0.05 or 0.10) into the A-site of $SrCoO_{3-\delta}$ resulted in a substantial increase of the electrical conductivity; for example, $Sm_{0.05}Sr_{0.95}CoO_{3-\delta}$ and $Sm_{0.1}Sr_{0.9}CoO_{3-\delta}$ exhibited maximum conductivity of 380 and 500 S cm^{-1}, respectively, which were more than 10 times that of the undoped $SrCoO_{3-\delta}$ parent oxide. Such substantial increase is due to the effective stabilization of oxygen-vacancy disordered perovskite structure. Figure 5b presents the conductivity curves of the **S−II**, **S−III**, **S−IV**, and **S−VI** bar-shaped samples, which provide information about the phase reaction and nature of the perovskite phase in the composite. For the **S−II** sample, the conductivity remains less than 1.0 S cm^{-1} even at 900 °C. Once the $SrCO_3$ and Co_3O_4 contents in the precursor increased to 20 and 10.89 wt %, respectively, the conductivity sharply increased for the membrane, reaching a maximum value of 13.8 S cm^{-1} at 550 °C, which is even higher than that of pure $SrCoO_{3-\delta}$ oxide at the same temperature (8.06 S cm^{-1}). This result is a strong sign of the formation of the highly conductive $Sm_xSr_{1-x}CoO_{3-\delta}$ phase in a percolating manner inside the membrane. The further increase in the $SrCO_3$ and Co_3O_4 contents in the membrane precursor envisioned a further increase in conductivity of the membrane, and a maximum value of 55 S cm^{-1} was reached for the **S−IV** sample at 550 °C. For the **S−VI** sample, it exhibited similar conductive behavior to the **S−III** sample. Above results further support the formation of a highly conductive perovskite phase $Sm_xSr_{1-x}CoO_{3-\delta}$ inside the membranes after the sintering at 1300 °C. However, the new perovskite phase only formed a percolating path when the $SrCO_3$ to SDC weight ratio reached 20:100 or higher in the precursor for the SDC + $SrCO_3$ + Co_3O_4 membranes. For the **S−III** sample, assuming the final composition after the sintering is SDC + $Sm_{0.05}Sm_{0.95}CoO_{3-\delta}$, as demonstrated by XRD, the volumetric ratio of the electronic conducting perovskite phase was calculated to be approximately 28%, which is in good agreement with the limit for the formation of a percolating phase.

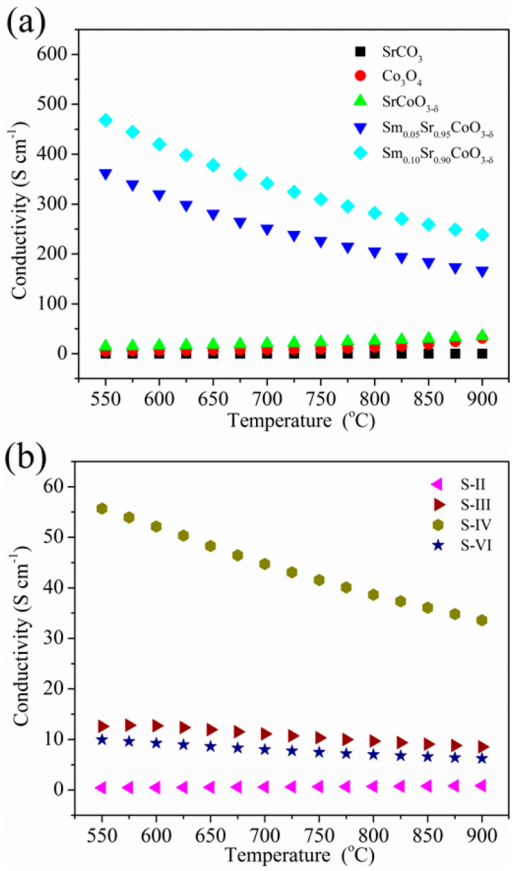

Figure 5. Electrical conductivity of $SrCO_3$, Co_3O_4, $SrCoO_{3-\delta}$, $Sm_{0.05}Sr_{0.95}CoO_{3-\delta}$, $Sm_{0.1}Sr_{0.9}CoO_{3-\delta}$ (a) and SDC + 10 wt % $SrCO_3$ + 5.44 wt % Co_3O_4 (**S−II**), SDC + 20 wt % $SrCO_3$ + 10.89 wt % Co_3O_4 (**S−III**), SDC + 40 wt % $SrCO_3$ + 21.76 wt % Co_3O_4 (**S−IV**), SDC + 26.36 wt % $SrCoO_{3-\delta}$ (**S−VI**) (b) in the temperature range of 550−900 °C.

As a ceramic membrane for oxygen separation, a high oxygen bulk diffusion rate and fast oxygen surface exchange kinetics are crucial to achieving high oxygen permeability. The formation of $Sm_xSr_{1-x}CoO_{3-\delta}$ perovskite in a percolating manner in the membranes should benefit the oxygen ion diffusion and oxygen surface exchange because such an oxygen-vacancy-disordered perovskite possesses a high oxygen ion conductivity and surface exchange coefficient.[43] Thus, the **S−III** bar-shaped pellets were then subjected to electrical conductivity relaxation measurements at 650, 700, 750, 800, and 850 °C to obtain information about their chemical diffusion and surface chemical exchange coefficients. Shown in Figure 6 are the typical relaxation curves for the **S−III** sample at various temperatures. The short time (less than 700 s even at 650 °C) for the conductivity to reach a new equilibrium after the sudden change of the surrounding atmosphere with the oxygen partial pressure increasing from 0.1 to 0.21 atm implies the good bulk diffusion and surface exchange kinetics. Both the D_{chem} and κ_{chem} values were derived by mathematic modeling of the relaxation curves based on Fick's diffusion equation,[44,45] which was described in detail in our previous publiacation.[35] Listed in Table 2 are the derived D_{chem} and κ_{chem} at the five temperatures. High D_{chem} and κ_{chem} values were obtained for **S−III** membranes, which are comparable to those of many highly active mixed conducting oxides. For example, LSCF was reported to exhibit D_{chem} and κ_{chem} values of 1.0×10^{-5} cm^2 s^{-1} and 1.5×10^{-3} cm s^{-1} at 800 °C,[46] as measured by the similar ECR technique; for comparison, the **S−III** sample exhibited D_{chem} and κ_{chem} values of 2.42×10^{-4} cm^2 s^{-1} and 2.48×10^{-3} cm s^{-1}, respectively, at the same temperature. For comparison, the corresponding

DOI: 10.1021/acsami.5b05812
ACS Appl. Mater. Interfaces 2015, 7, 22918−22926

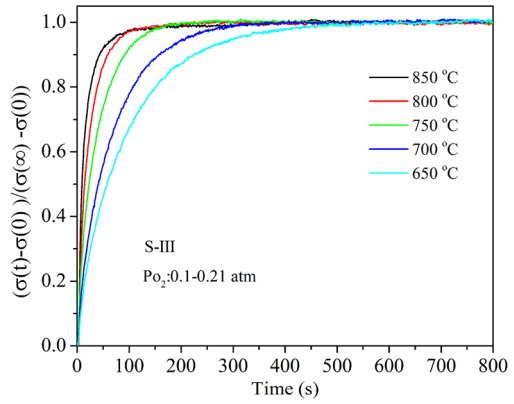

Figure 6. ECR response curves of SDC + 20 wt % $SrCO_3$ + 10.89 wt % Co_3O_4 (**S−III**) at various temperatures after the sudden change of oxygen partial pressure of the surrounding atmosphere from 0.1 to 0.21 atm.

Table 2. D_{chem} and κ_{chem} at Various Temperatures for SDC + 20 wt % $SrCO_3$ + 10.89 wt % Co_3O_4 (S−III) Bar-Shaped Pellet

T (° C)	650	700	750	800	850
$D_{chem} \times 10^4$ (cm^2 s^{-1})	0.58	0.83	1.46	2.42	3.66
$k_{chem} \times 10^3$ (cm s^{-1})	0.57	0.83	1.44	2.48	3.81

values of the **S−VI** sample (Figure S3) were also measured by the same ECR technique and are presented in Table S2. In addition, the D_{chem} and κ_{chem} values of both **S−III** and **S−VI** membranes are very comparable, which further suggests the feasibility of the fabrication of the dual-phase membrane through beneficial phase reaction.

3.4. Oxygen Permeation. The oxygen permeability of the as-fabricated dual-phase membranes by the beneficial phase reaction was then investigated based on the oxygen permeation flux through the membranes under a gradient of air/helium. For comparison purposes, **S−VII**, **S−VIII**, and pure SDC membranes were also fabricated, and their permeation fluxes were also measured. Figure 7 shows the temperature dependence of the oxygen permeation fluxes through **S−II**, **S−III**, **S−IV**, **S−VII**, **S−VIII**, and SDC membranes. All the membrane

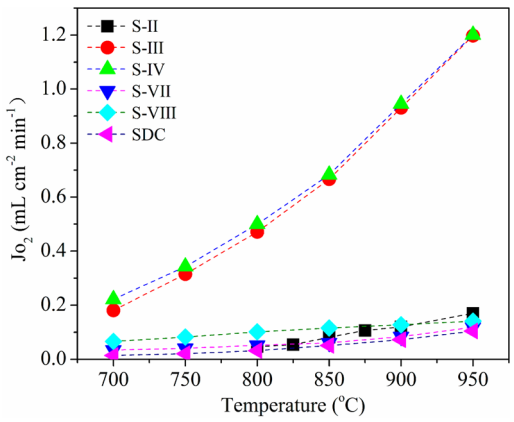

Figure 7. Temperature dependence of the oxygen permeation fluxes through SDC + 10 wt % $SrCO_3$ + 5.44 wt % Co_3O_4 (**S−II**), SDC + 20 wt % $SrCO_3$ + 10.89 wt % Co_3O_4 (**S−III**), SDC + 40 wt % $SrCO_3$ + 21.76 wt % Co_3O_4 (**S−IV**), SDC + 20 wt % $SrCO_3$ (**S−VII**), SDC + 10.89 wt % Co_3O_4 (**S−VIII**), and SDC membranes.

thicknesses were fixed at 0.5 mm. For the pure SDC membrane, a negligible oxygen permeation flux was obtained at temperatures lower than 800 °C, and the value was still only 0.07 mL cm^{-2} min^{-1} [STP] even at 900 °C. Such low oxygen permeation fluxes are closely related to the low electronic conductivity of the SDC phase. For the **S−VII** and **S−VIII** membranes, their permeation fluxes were also small, reaching only 0.083 and 0.13 mL cm^{-2} min^{-1} [STP] at 900 °C, respectively. It suggests the importance of the in situ formed mixed conducting perovskite phase for achieving high oxygen permeation of the membranes. The **S−II** membrane also exhibited relatively low oxygen permeation fluxes, for example, reaching only 0.13 mL cm^{-2} min^{-1} [STP] at 900 °C. In combination with the previous conductivity results, this unfavorable oxygen permeability of the **S−II** membrane can be explained by the failure of the creation of percolating electronic conducting paths inside the membrane. For the **S−III** membrane, the oxygen permeation flux was substantially increased compared with those of the previous measured membranes. For example, the flux reached 0.93 mL cm^{-2} min^{-1} [STP] at 900 °C, which is almost 8 times that of the **S−II** membrane. The formation of a percolating perovskite phase inside the membrane significantly improved the apparent electronic conductivity, and thus, the simultaneous diffusion of oxygen ions and electrons through the membrane become applicable, leading to a substantial increase in the oxygen permeation flux. Notably, after the perovskite phase reached the threshold for percolation, the further increase in the content of raw materials for the perovskite phase did not result in a further increase in oxygen permeation flux. It implies that under such conditions, the oxygen conductivity played a more important role in determining the oxygen permeation flux, while the perovskite oxide likely had similar oxygen-ion conductivity to that of the SDC phase. Thus, a further increase in the weight ratio of the perovskite phase did not help to further increase the permeation flux. As to the **S−VI** membrane (shown in Figure S4), the oxygen permeation fluxes were slightly lower than the **S−III** membrane, which may be due to the formed K_2NiF_4-type phase $Sm_{2-x}Sr_xCoO_{4+\delta}$ after sintered at 1200 °C.

It is well-known that the oxygen permeation through a mixed conducting membrane could be rate determined by slow oxygen-bulk diffusion, slow electron diffusion, slow surface exchange or a combination of these processes. The rate determination step of the **S−III** membrane was investigated by measuring the oxygen permeation fluxes of several membrane pellets with different thicknesses under an air/helium gradient. During the measurement, the helium flow rate was fixed at 100 mL min^{-1} [STP]. If the oxygen permeation process was rate determined by the slow surface kinetics, the membrane permeation flux would remain unchanged with variation of the membrane thickness. However, a reverse proportional relationship of the oxygen permeation flux to the membrane thickness was expected if the membrane flux was fully bulk diffusion controlled and the oxygen gradient across the membrane kept unchanged. Figure 8a shows the oxygen permeation fluxes of four **S−III** membranes with different thicknesses of 0.4, 0.5, 0.75, and 1.00 mm in the temperature range of 700−950 °C. An increase in the oxygen permeation flux with a decrease of the membrane thickness was observed, which strongly demonstrated the significant role of bulk diffusion in the rate determination of oxygen permeation through the **S−III** membrane if the membrane thickness was in the range of 0.4−1.0 mm. Figure 8b presents the $Jo_2 \times d$ (d was

DOI: 10.1021/acsami.5b05812
ACS Appl. Mater. Interfaces 2015, 7, 22918−22926

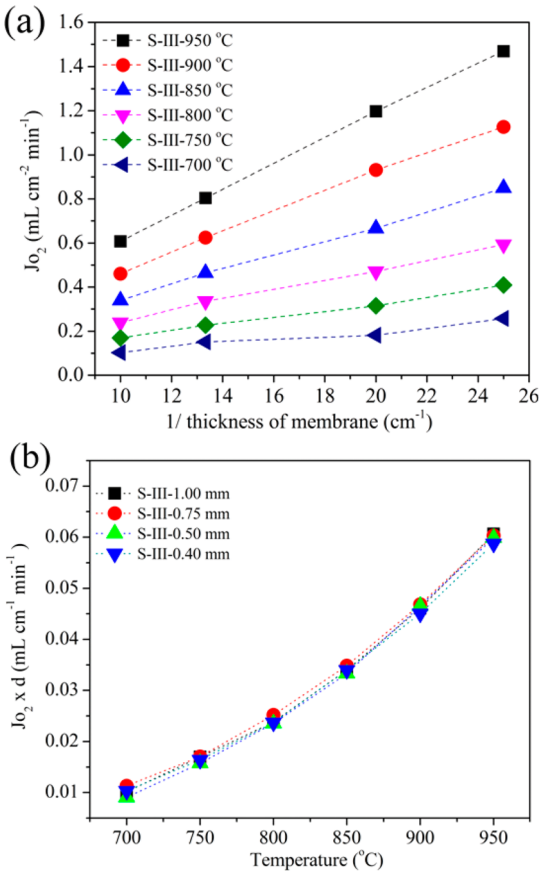

Figure 8. (a) The oxygen permeation fluxes through the SDC + 20 wt % $SrCO_3$ + 10.89 wt % Co_3O_4 (**S−III**) membrane as a function of the thickness for the different temperature. (b) $Jo_2 \times d$ versus temperature curves of the four SDC + 20 wt % $SrCO_3$ + 10.89 wt % Co_3O_4 (**S−III**) membranes with different thicknesses.

the thickness of membrane) versus temperature curves of the four **S−III** membranes with different thicknesses. The almost overlapped curves further supported the oxygen permeation being largely determined by the slow oxygen bulk diffusion process. For the **S−III** membrane, the electron diffusion was less likely to be the rate-determining step because a much higher electronic conductivity was expected than the oxygen ionic conductivity after the formation of the percolating perovskite phase in the composite membrane. Thus, the oxygen bulk diffusion should be the main rate-determining step for oxygen permeation through the **S−III** membrane. It should be noted that due to the fixed helium flow rate, the oxygen partial pressure of the oxygen lead side membrane surface was slightly different for the various membranes with different thicknesses, which should have somewhat affected the oxygen permeation fluxes of the membrane. Thus, the partial role of oxygen surface exchange in the rate determination is still possible even though the $J_{O_2} \times d$ versus temperature curves for the four membranes were well overlapped.

A stable oxygen permeation process is an important requirement of the ceramic membrane for oxygen separation. In particular, CO_2 poisoning is a big problem for many alkaline-earth-containing perovskite membranes. Here pure CO_2 was selected as the sweep gas to test the oxygen permeation stability of the membrane. Figure 9 presents the response of the oxygen permeation flux of **S−III** membrane with respect to time on a CO_2 stream for a total period of 110 h at 900 °C. After a

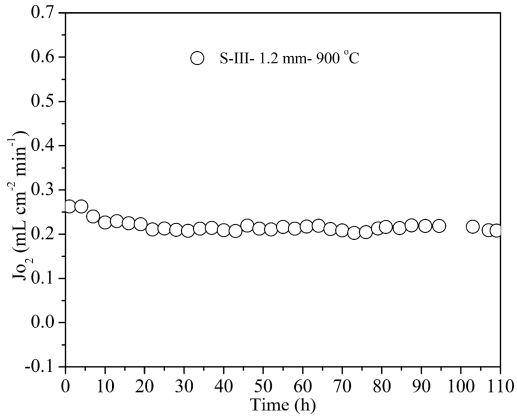

Figure 9. Long-time oxygen permeation behavior of a SDC + 20 wt % $SrCO_3$ + 10.89 wt % Co_3O_4 (**S−III**) membrane with a membrane thickness of 1.2 mm at 900 °C with air as oxygen-rich side atmosphere and CO_2 as sweep gas.

modest drop in the permeation flux during the initial 10 h, a fairly stable oxygen permeation flux was reached in the following 100 h of the test, demonstrating the favorable stability of the membrane for oxygen separation. It thus promises the beneficial phase reaction to be a practical method for the development of high-performance dual-phase ceramic membranes.

4. CONCLUSIONS

In this study, we reported a novel approach for the development of dual-phase composite membranes for oxygen separation with favorable oxygen permeability and stability by utilizing the beneficial solid-state reaction at high temperature. The phase reaction occurred between the fluorite phases (SDC) and raw materials ($SrCO_3$ + Co_3O_4) for pervoskite phase, forming the highly conductive tetragonal pervoskite phase $Sm_xSr_{1-x}CoO_{3-\delta}$. The BSEM analysis and conductivity of the as-sintered samples reveal that the element percolation is in a three-dimensional manner. The oxygen permeability and stability of the various SDC + $SrCO_3$ + Co_3O_4 membranes were investigated systematically, and SDC + 20 wt % $SrCO_3$ + 10.89 wt % Co_3O_4 membrane exhibited the highest oxygen permeation flux. Under an air/helium gradient, the permeation flux through a 0.5 mm-thick SDC + 20 wt % $SrCO_3$ + 10.89 wt % Co_3O_4 membrane reached 1.19 and 0.17 mL cm^{-2} min^{-1} [STP] at 950 and 700 °C, respectively. Moreover, the dual-phase membrane could maintain a stable oxygen permeation flux during the 110 h permeation test with pure CO_2 as the sweep gas. All these results demonstrate that this innovative beneficial phase reaction technique has the potential in high-performance ceramic membranes for oxygen separation, and may also be applicable for the preparation of other functional composites.

■ ASSOCIATED CONTENT

Supporting Information

The Supporting Information is available free of charge on the ACS Publications website at DOI: 10.1021/acsami.5b05812.

XRD patterns of SDC, $SrCoO_{3-\delta}$, fresh SDC + 26.36 wt % $SrCoO_{3-\delta}$ mixture after ball-milling without sintering and SDC + 26.36 wt % $SrCoO_{3-\delta}$ membrane after sintered at 1200 °C; XRD patterns with Rietveld refinement plots of $Sm_xSr_{1-x}CoO_{3-\delta}$ and SDC + 26.36

DOI: 10.1021/acsami.5b05812
ACS Appl. Mater. Interfaces 2015, 7, 22918−22926

wt % $SrCoO_{3-\delta}$; chemical composition of as-prepared membranes; the ECR response curves and temperature dependence of the oxygen permeation fluxes of SDC + 26.36 wt % $SrCoO_{3-\delta}$ sample. (PDF)

AUTHOR INFORMATION

Corresponding Author

*E-mail: shaozp@njtech.edu.cn. Tel.: +86 25 83172256. Fax: +86 25 83172242.

Notes

The authors declare no competing financial interest.

ACKNOWLEDGMENTS

This work was financially supported by the Key Projects in Nature Science Foundation of Jiangsu Province under Contract No. BK2011030 and by the Priority Academic Program Development of Jiangsu Higher Education Institutions and the Program for Jiangsu Specially-Appointed Professors.

REFERENCES

(1) Leo, A.; Liu, S. M.; da Costa, J. C. D. Development of mixed conducting membranes for clean coal energy delivery. *Int. J. Greenhouse Gas Control* **2009**, *3*, 357−367.

(2) Partovi, K.; Liang, F. Y.; Ravkina, O.; Caro, J. High-Flux Oxygen-Transporting Membrane $Pr_{0.6}Sr_{0.4}Co_{0.5}Fe_{0.5}O_{3-\delta}$: CO_2 Stability and Microstructure. *ACS Appl. Mater. Interfaces* **2014**, *6*, 10274−10282.

(3) Lobera, M. P.; Serra, J. M.; Foghmoes, S. P.; Sogaard, M.; Kaiser, A. On the use of supported ceria membranes for oxyfuel process/syngas production. *J. Membr. Sci.* **2011**, *385*, 154−161.

(4) Søgaard, M.; Hendriksen, P. V.; Mogensen, M. Oxygen nonstoichiometry and transport properties of strontium substituted lanthanum ferrite. *J. Solid State Chem.* **2007**, *180*, 1489−1503.

(5) Schulz, M.; Pippardt, U.; Kiesel, L.; Ritter, K.; Kriegel, R. Oxygen permeation of various archetypes of oxygen membranes based on BSCF. *AIChE J.* **2012**, *58*, 3195−3202.

(6) Dalslet, B. T.; Søgaard, M.; Hendriksen, P. V. Defect chemistry and oxygen transport of $(La_{0.6}Sr_{0.4-x}M_x)_{0.99}Co_{0.2}Fe_{0.8}O_{3-\delta}$, M = Ca(x = 0.05, 0.1), Ba (x= 0.1, 0.2), Sr: Part II: Oxygen transport. *Solid State Ionics* **2009**, *180*, 1050−1060.

(7) Chen, C. S.; Feng, S. J.; Ran, S.; Zhu, D. C.; Liu, W.; Bouwmeester, H. J. Conversion of Methane to Syngas by a Membrane-Based Oxidation-Reforming Process. *Angew. Chem., Int. Ed.* **2003**, *42*, 5196−5198.

(8) Wang, Z. T.; Sun, W. P.; Zhu, Z. W.; Liu, T.; Liu, W. A Novel Cobalt-Free, CO_2-Stable, and Reduction-Tolerant Dual-Phase Oxygen-Permeable Membrane. *ACS Appl. Mater. Interfaces* **2013**, *5*, 11038−11043.

(9) Wang, H.; Tablet, C.; Feldhoff, A.; Caro, J. A Cobalt-Free Oxygen-Permeable Membrane Based on the Perovskite-Type Oxide $Ba_{0.5}Sr_{0.5}Zn_{0.2}Fe_{0.8}O_{3-\delta}$. *Adv. Mater.* **2005**, *17*, 1785−1788.

(10) Liu, T.; Wang, Y.; Yuan, R. H.; Gao, J. F.; Chen, C. S.; Bouwmeester, H. J. M. Enhancing the Oxygen Permeation Rate of $Zr_{0.84}Y_{0.16}O_{1.92}$-$La_{0.8}Sr_{0.2}Cr_{0.5}Fe_{0.5}O_{3-\delta}$ Dual-Phase Hollow Fiber Membrane by Coating with $Ce_{0.8}Sm_{0.2}O_{1.9}$ Nanoparticles. *ACS Appl. Mater. Interfaces* **2013**, *5*, 9454−9460.

(11) Shao, Z. P.; Yang, W. S.; Cong, Y.; Dong, H.; Tong, J. H.; Xiong, G. X. Investigation of the permeation behavior and stability of a $Ba_{0.5}Sr_{0.5}Co_{0.8}Fe_{0.2}O_{3-\delta}$ oxygen membrane. *J. Membr. Sci.* **2000**, *172*, 177−188.

(12) Ruiz-Trejo, E.; Boldrin, P.; Medley-Hallam, J. L.; Darr, J.; Atkinson, A.; Brandon, N. P. Partial oxidation of methane using silver/gadolinia-doped ceria composite membranes. *Chem. Eng. Sci.* **2015**, *127*, 269−275.

(13) Zhu, X. F.; Liu, H. Y.; Cong, Y.; Yang, W. S. Novel dual-phase membranes for CO_2 capture *via* an oxyfuel route. *Chem. Commun.* **2012**, *48*, 251−253.

(14) Sunarso, J.; Liu, S.; Lin, Y. S.; da Costa, J. C. D. Oxygen permeation performance of $BaBiO_{3-\delta}$ ceramic membranes. *J. Membr. Sci.* **2009**, *344*, 281−287.

(15) Ruiz-Trejo, E.; Boldrin, P.; Lubin, A.; Tariq, F.; Fearn, S.; Chater, R.; Cook, S. N.; Atkinson, A.; Gruar, R. I.; Tighe, C. J.; Brandon, N. P. Novel Composite Cermet for Low-Metal-Content Oxygen Separation Membranes. *Chem. Mater.* **2014**, *26*, 3887−3895.

(16) Wu, K.; Xie, S.; Jiang, G. S.; Chen, C. S. Oxygen permeation through $(Bi_2O_3)_{0.74}(SrO)_{0.26}$-Ag(40% v/o) composite. *J. Membr. Sci.* **2001**, *188*, 189−193.

(17) Kobayashi, K.; Tsunoda, T. Oxygen permeation and electrical transport properties of 60 vol.% $Bi_{1.6}Y_{0.4}O_3$ and 40 vol.% Ag composite prepared by the sol−gel method. *Solid State Ionics* **2004**, *175*, 405−408.

(18) Zhang, Z. B.; Chen, Y. B.; Tade, M. O.; Hao, Y.; Liu, S. M.; Shao, Z. P. Tin-doped perovskite mixed conducting membrane for efficient air separation. *J. Mater. Chem. A* **2014**, *2*, 9666−9674.

(19) Zeng, P. Y.; Shao, Z. P.; Liu, S. M.; Xu, Z. P. Influence of M cations on structural, thermal and electrical properties of new oxygen selective membranes based on $SrCo_{0.95}M_{0.05}O_{3-\delta}$ perovskite. *Sep. Purif. Technol.* **2009**, *67*, 304−311.

(20) Chen, D. J.; Chen, C.; Zhang, Z. B.; Baiyee, Z. M.; Ciucci, F. Compositional Engineering of Perovskite Oxides for Highly Efficient Oxygen Reduction Reactions. *ACS Appl. Mater. Interfaces* **2015**, *7*, 8562−8571.

(21) Dong, F. F.; Chen, D. J.; Ran, R.; Park, H.; Kwak, C.; Shao, Z. P. A comparative study of $Sm_{0.5}Sr_{0.5}MO_{3-\delta}$ (M= Co and Mn) as oxygen reduction electrodes for solid oxide fuel cells. *Int. J. Hydrogen Energy* **2012**, *37*, 4377−4387.

(22) Kim, S.; Yang, Y. L.; Christoffersen, R.; Jacobson, A. J. Oxygen permeation, electrical conductivity and stability of the perovskite oxide $La_{0.2}Sr_{0.8}Cu_{0.4}Co_{0.6}O_{3-x}$. *Solid State Ionics* **1997**, *104*, 57−65.

(23) Zhang, Z. B.; Chen, D. J.; Chen, Y. B.; Hao, Y.; Tade, M. O.; Shao, Z. P. Facile fabrication and improved carbon dioxide tolerance of a novel bilayer-structured ceramic oxygen permeating membrane. *J. Membr. Sci.* **2014**, *472*, 10−18.

(24) Sun, M.; Chen, X. W.; Hong, L. Influence of the Interfacial Phase on the Structural Integrity and Oxygen Permeability of a Dual-Phase Membrane. *ACS Appl. Mater. Interfaces* **2013**, *5*, 9067−9074.

(25) Li, W.; Liu, J. J.; Chen, C. S. Hollow fiber membrane of yttrium-stabilized zirconia and strontium-doped lanthanum Manganite dual-phase composite for oxygen separation. *J. Membr. Sci.* **2009**, *340*, 266−271.

(26) Luo, H. X.; Efimov, K.; Jiang, H. Q.; Feldhoff, A.; Wang, H. H.; Caro, J. CO_2-Stable and Cobalt-Free Dual-Phase Membrane for Oxygen Separation. *Angew. Chem., Int. Ed.* **2011**, *50*, 759−763.

(27) Zhu, X. F.; Li, Q. M.; He, Y. F.; Cong, Y.; Yang, W. Oxygen permeation and partial oxidation of methane in dual-phase membrane reactors. *J. Membr. Sci.* **2010**, *360*, 454−460.

(28) Luo, H. X.; Jiang, H. Q.; Klande, T.; Cao, Z. W.; Liang, F. Y.; Wang, H. H.; Caro, J. Novel Cobalt-Free, Noble Metal-Free Oxygen-Permeable $40Pr_{0.6}Sr_{0.4}FeO_{3-\delta}$-$60Ce_{0.9}Pr_{0.1}O_{2-\delta}$ Dual-Phase Membrane. *Chem. Mater.* **2012**, *24*, 2148−2154.

(29) Wang, B.; Zhan, M. C.; Zhu, D. C.; Liu, W.; Chen, C. S. Oxygen permeation and stability of $Zr_{0.8}Y_{0.2}O_{0.9}$-$La_{0.8}Sr_{0.2}CrO_{3-\delta}$ dual-phase composite. *J. Solid State Electrochem.* **2006**, *10*, 625−628.

(30) Liu, J. J.; Liu, T.; Wang, W. D.; Gao, J. F.; Chen, C. S. $Zr_{0.84}Y_{0.16}O_{1.92}$-$La_{0.8}Sr_{0.2}Cr_{0.5}Fe_{0.5}O_{3-\delta}$ dual-phase composite hollow fiber membrane targeting chemical reactor applications. *J. Membr. Sci.* **2012**, *389*, 435−440.

(31) Luo, H. X.; Jiang, H. Q.; Efimov, K.; Caro, J.; Wang, H. H. Influence of the preparation methods on the microstructure and oxygen permeability of a CO_2-stable dual phase membrane. *AIChE J.* **2011**, *57*, 2738−2745.

(32) Li, Q. M.; Zhu, X. F.; He, Y. F.; Cong, Y.; Yang, W. S. Effects of sintering temperature on properties of dual-phase oxygen permeable membranes. *J. Membr. Sci.* **2011**, *367*, 134−140.

(33) Chen, D. J.; Yang, G. M.; Ciucci, F.; Tade, M. O.; Shao, Z. P. 3D core-shell architecture from infiltration and beneficial reactive sintering

DOI: 10.1021/acsami.5b05812
ACS Appl. Mater. Interfaces 2015, 7, 22918−22926

as highly efficient and thermally stable oxygen reduction electrode. *J. Mater. Chem. A* **2014**, *2*, 1284−1293.
(34) Zhang, K.; Shao, Z. P.; Li, C. Z.; Liu, S. M. Novel CO_2-tolerant ion-transporting ceramic membranes with an external short circuit for oxygen separation at intermediate temperatures. *Energy Environ. Sci.* **2012**, *5*, 5257−5264.
(35) Chen, D. J.; Shao, Z. P. Surface exchange and bulk diffusion properties of $Ba_{0.5}Sr_{0.5}Co_{0.8}Fe_{0.2}O_{3-\delta}$ mixed conductor. *Int. J. Hydrogen Energy* **2011**, *36*, 6948−6956.
(36) Zhang, Z. B.; Chen, D. J.; Gao, Y.; Yang, G. M.; Dong, F. F.; Ciucci, F.; Shao, Z. P. A CO_2-tolerant nanostructured layer for oxygen transport membranes. *RSC Adv.* **2014**, *4*, 25924−25932.
(37) Ciucci, F. Electrical conductivity relaxation measurements: Statistical investigations using sensitivity analysis, optimal experimental design and ECRTOOLS. *Solid State Ionics* **2013**, *239*, 28−40.
(38) Chen, Y. B.; Qian, B. M.; Yang, G. M.; Chen, D. J.; Shao, Z. P. Insight into an unusual lanthanum effect on the oxygen reduction reaction activity of Ruddlesden-Popper-type cation-nonstoichiometric $La_{2-x}NiO_{4+\delta}$ (x = 0−0.1) oxides. *J. Mater. Chem. A* **2015**, *3*, 6501−6508.
(39) Nicholas, J. D.; De Jonghe, L. C. Prediction and evaluation of sintering aids for cerium gadolinium oxide. *Solid State Ionics* **2007**, *178*, 1187−1194.
(40) Fagg, D. P.; Kharton, V. V.; Frade, J. R. P-type electronic transport in $Ce_{0.8}Gd_{0.2}O_{2-\delta}$: the effect of transition metal oxide sintering aids. *J. Electroceram.* **2002**, *9*, 199−207.
(41) Fagg, D. P.; Abrantes, J. C. C.; Perez-Coll, D.; Nunez, P.; Kharton, V. V.; Frade, J. R. The effect of cobalt oxide sintering aid on electronic transport in $Ce_{0.80}Gd_{0.20}O_{2-\delta}$ electrolyte. *Electrochim. Acta* **2003**, *48*, 1023−1029.
(42) Bodén, A.; Di, J.; Lagergren, C.; Lindbergh, G.; Wang, C. Y. Conductivity of SDC and $(Li/Na)_2CO_3$ composite electrolytes in reducing and oxidising atmospheres. *J. Power Sources* **2007**, *172*, 520−529.
(43) Dong, F. F.; Chen, Y. B.; Chen, D. J.; Shao, Z. P. Surprisingly High Activity for Oxygen Reduction Reaction of Selected Oxides Lacking Long Oxygen-Ion Diffusion Paths at Intermediate Temperatures: A Case Study of Cobalt-Free $BaFeO_{3-\delta}$. *ACS Appl. Mater. Interfaces* **2014**, *6*, 11180−11189.
(44) Balaguer, M.; Solís, C.; Serra, J. M. Study of the Transport Properties of the Mixed Ionic Electronic Conductor $Ce_{1-x}Tb_xO_{2-\delta}$+Co (x= 0.1, 0.2) and Evaluation as Oxygen-Transport Membrane. *Chem. Mater.* **2011**, *23*, 2333−2343.
(45) Søgaard, M.; Hendriksen, P. V.; Mogensen, M. Oxygen nonstoichiometry and transport properties of strontium substituted lanthanum ferrite. *J. Solid State Chem.* **2007**, *180*, 1489−1503.
(46) Katsuki, M.; Wang, S. R.; Dokiya, M.; Hashimoto, T. High temperature properties of $La_{0.6}Sr_{0.4}Co_{0.8}Fe_{0.2}O_{3-\delta}$ oxygen nonstoichiometry and chemical diffusion constant. *Solid State Ionics* **2003**, *156*, 453−461.

DOI: 10.1021/acsami.5b05812
ACS Appl. Mater. Interfaces 2015, 7, 22918−22926